Available online at www.sciencedirect.com

ScienceDirect

Procedia Structural Integrity 64 (2024) 426–435

Structural Integrity Procedia

www.elsevier.com/locate/procedia

SMAR 2024 – 7th International Conference on Smart Monitoring, Assessment and Rehabilitation of Civil Structures

Innovative hybrid CFRP composite and Fe-SMA bonded systems for structural glass flexural strengthening

Jorge Rocha[a], Eduardo Pereira[a], José Sena-Cruz[a]*

[a]*ISISE/ARISE, University of Minho, 4800-058 Guimarães, Portugal*

Abstract

Contemporary architecture is increasingly embracing the use of structural glass for challenging applications. Glass industry has been adopting thermal toughening and lamination as advanced techniques to enhance tensile strength and avoid sudden failures. However, unexpected failure persists and hinders a more widespread application of glass, including as a structural material. Researchers have tested alternative glass composite systems, integrating reinforcements like steel, fiber-reinforced polymers (FRP), or iron-based shape memory alloy (Fe-SMA). This study explores an innovative concept that involves the simultaneous application of CFRP and Fe-SMA reinforcements via near-surface mounted (NSM) or externally bonded reinforced (EBR) techniques for glass strengthening. This system is shown to effectively prevent premature debonding, enhance post-cracking response, and ensure ductile failure modes, while being simple. Bending tests on large-scale laminated glass beams were performed to characterize the effectiveness of the system, while also the benefits of post-tensioning were investigated by inducing different prestressing levels in the glass strengthened elements. The paper first highlights the advantages of Fe-SMA reinforcements in glass composite systems through experimental evidence, followed by exploration of the proposed innovative hybrid CFRP composite and Fe-SMA bonded systems.

Keywords: Structural glass beams; Hybrid strengthening system; CFRP; Fe-SMA

1. Introduction

Unlike other load-bearing materials, glass is prone to unexpected failure (e.g. NiS inclusions) even without any discernible fault in the design process. Moreover, localized failures in glass can precipitate the complete collapse of a

* Corresponding author
E-mail address: jose.sena-cruz@civil.uminho.pt

10.1016/j.prostr.2024.09.279

structure, even under loads below those anticipated for the Ultimate Limit State (ULS). In contrast to reinforced concrete, where cracking is acceptable in service, the breakage of glass invariably leads to structural collapse. Consequently, to mitigate these risks, design methodologies tend to result in over-designed solutions such as the incorporation of sacrificial sheets in laminated glass panels. However, these approaches inflate construction costs and diverge from sustainable building practices (Martens *et al.* 2015).

Among the few design standards governing structural glass applications (e.g., CNR-DT 2010/2013, prCEN/TS 19100-1:2021), there is a growing emphasis on additional verifications concerning post-cracking performance. These verifications serve two primary purposes: (i) ensuring the safety of individuals and structures during a cracking event, such as preventing the dislodging of fragments (Wüest *et al.* 2021), and (ii) verifying that glass components retain the ability to support a portion of the loads anticipated for ULS conditions (i.e., residual load-carrying capacity). An established method to promote relatively ductile failure mechanisms involves the adhesive bonding and/or mechanical anchoring of multiple load-bearing materials. In the event of material fracture, these reinforcements can sustain residual strength and stiffness (Valarinho *et al.* 2013). Various reinforcement materials, including timber (e.g., Cruz et al. 2008), steel (e.g., Louter *et al.* 2021), Carbon Fibre Reinforced Polymers (CFRP) (e.g., Jordão *et al.* 2014), and Glass Fibre Reinforced Polymers (GFRP) (e.g., Veer *et al.* 2011), have been explored for their potential in enhancing the structural integrity of glass.

Like prestressing techniques employed in concrete structures, post-tensioned composite systems have garnered recent attention from the scientific community. The objective is to improve the performance of glass structural elements, enabling the creation of thinner profiles to enhance transparency, lower the cost of glass buildings, and align with contemporary environmental objectives. Post-tensioned glass systems have been developed utilizing various reinforcements, including steel (e.g., Jordão *et al.* 2014), CFRP (e.g., Louter *et al.* 2014), or SMA (e.g., Silvestru *et al.* 2022). In contrast to tempering, post-tensioning offers several advantages: (i) the post-failure performance of glass remains largely unaffected; (ii) glass theoretically retains the ability to be drilled or cut post-tensioning; (iii) tailored prestressing levels and layouts can be implemented for each structural element based on its specific loading conditions; and, (iv) in the event of glass rupture, the reinforcement bridges cracks, transferring tensile forces to the supports and providing residual load-carrying capacity. Nonetheless, a significant challenge in post-tensioning lies in effectively transferring the prestressing force from the reinforcement to the glass.

Considering the aforementioned factors, Shape Memory Alloys (SMAs) stand out as a promising reinforcement material for the development of post-tensioned glass systems. This potential is derived from the adhesive damage gradient generated through temperature exposure during SMA activation. In the realm of concrete structures, SMAs have demonstrated utility in enhancing damping during seismic events (e.g., Asgarian *et al.* 2011) and in post-tensioned strengthening applications (e.g., Hosseini *et al.* 2019). Despite the growing interest in glass-SMA composite systems, few studies are found in the literature. Previous investigations have centered on assessing the bond behavior of glass-to-SMA adhesively bonded joints (e.g., Silvestru *et al.* 2022). However, Silvestru *et al.* 2022 pioneered the exploration of Fe-SMA reinforcement activation for post-tensioning laminated glass beams, aiming to ensure additional load-carrying capacity following glass breakage.

This study investigates the viability of post-tensioning monolithic glass beams through the activation of externally bonded Fe-SMA reinforcement. Additionally, it explores the advantages of employing Fe-SMA reinforcement to create hybrid strengthening systems capable of enhancing the overall performance of glass elements. The experimental framework includes: (i) mechanical characterization tests on adhesives and Fe-SMA; (ii) four-point bending tests on small-scale and monolithic glass beams to evaluate the impact of activating SMA reinforcement on the initial cracking load and post-cracking behavior; and, (iii) flexural tests on large-scale laminated glass beams to determine the optimal hybrid strengthening configuration for enhancing overall structural response.

2. Materials, specimens, and test methods

2.1. Glass, Fe-SMA and CFRP

The mechanical properties of glass, adhesives and reinforcement materials adopted in this research were already assessed in previous studies (Rocha *et al.* 2022a, 2022b, 2023).

Annealed glass was used in these experiments to improve the post-failure performance. Its mechanical properties are shown in Table 1, like tensile strength ($f_{g,t}$), modulus of elasticity (E_g), ultimate strain ($\varepsilon_{r,ult}$) and Poisson's ratio (υ).

For reinforcement, Fe-SMA commercialized by re-fer AG Company and CFRP laminates produced by S&P® Clever Reinforcement Company were used in this investigation. Mechanical properties were determined, for each reinforcement material, based on tensile tests on five coupons of 250 (length) × 10 (width) [mm] at a constant displacement rate of 1.0 mm/min, according to EN ISO 527-2:2012. Table 1 shows their E-modulus (E_r) and tensile strength (f_r). Unlike CFRP, with linear elastic behavior until failure, Fe-SMA presented an extensive yielding stage before failure, as depicted in Fig. 1.

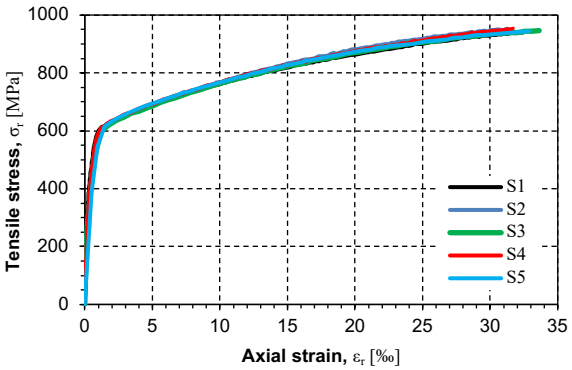

Fig. 1. Stress-strain curves obtained from the mechanical characterization tests on Fe-SMA.

The two-component epoxy adhesives SikaDur®-330 and 3M Scotch-Weld DP490 – later called as SD and 3M – were used to bond CFRP and Fe-SMA to the glass, respectively. Table 1 presents their E-modulus (E_{adh}), tensile strength ($f_{adh,t}$) and ultimate strain ($\varepsilon_{adh,ult}$), which were estimated according to EN ISO 527-2:2012. While SD adhesive exhibited linear elastic behavior until failure, 3M adhesive showed a slight loss of stiffness for increasing load.

Table 1. Mechanical properties (average values) of the Fe-SMA strips, CFRP laminates, annealed glass and 3M and SD adhesives (coefficients of variation, CoV, are indicated in parenthesis).

Material	E_r **[GPa]**	$f_{r,t}$ **[MPa]**	$\varepsilon_{r,ult}$ **[%]**	υ **[-]**
Fe-SMA	172.0 (1.7%)	948.1 (0.6%)	32.5 (2.3%)	0.39
CFRP	179.6 (1.9%)	2561.4 (2.9 %)	14.3 (3.6 %)	-
Material	E_g **[GPa]**	$f_{g,t}$ **[MPa]**	-	υ **[-]**
Annealed glass	8.4 (5.4%)	40	-	0.23
Material	E_{adh} **[MPa]**	$F_{adh,t}$ **[MPa]**	$\varepsilon_{adh,ult}$ **[‰]**	υ **[-]**
3M	1728.1 (3.3%)	32.8 (4.2%)	30.7 (2.8%)	0.38
SD	4325.3 (3.1%)	32.3 (3.9%)	8.4 (5.4%)	0.30

2.2. Beams

Two different series of beams were investigated in this work: (i) ***Series S1*** - monolithic glass panels externally reinforced with a Fe-SMA strip, and (ii) ***Series S2*** - laminated glass panels reinforced with combined EBR and NSM techniques. Monolithic beams, with a span of 1.4 m, were produced by externally bonding a Fe-SMA strip of 10 (width) × 1.5 (thickness) [mm] to the bottom edge of an annealed glass panel of 100 (height) × 12 (thickness) [mm] using the 3M adhesive. A total of 6 monolithic beams were manufactured: 2 reference beams (MB_T0), with passive Fe-SMA strips, and 4 post-tensioned beams (MB_Ti, with "i" being the activation temperature), with activated Fe-SMA strips. In addition, 2 laminated glass beams (LB_i-j, with "i" and "j" being the NSM and EBR reinforcement materials, respectively), with a span of 2.8 m, were manufactured according to the geometry shown in Fig. 2. They

consisted of joining three sheets of annealed glass using 1.52 mm thick PVB. As the inner layer is 22 mm smaller than the outer layers, a groove of 22 (depth) × 4.5 (thickness) [mm] was created for inserting the NSM reinforcement.

2.3. Fe-SMA activation

The activation of Fe-SMA reinforcement for post-tensioning the glass beams consisted of three typical phases, namely, pre-straining, heating and cooling.

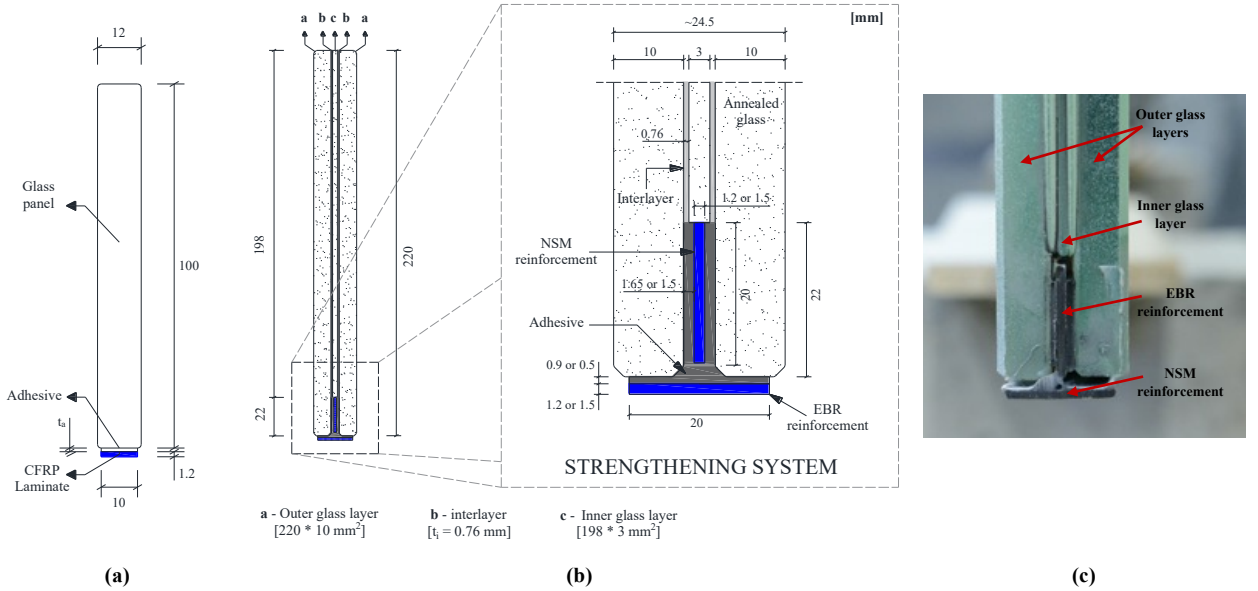

Fig. 2. Schematic representation of the cross section of (i) monolithic glass beams (series S1); (b) laminated glass beams (series S2); and (c) image showing the strengthening system adopted in Series S2. Units in [mm].

Based on the study carried out by Shahverdi *et al*. (2008), Fe-SMA strips were prestrained to 2.0 % at room temperature before being adhesively bonded to the glass. A prestrain of 2.0 % was proved to be sufficient to induce martensitic transformation and take full advantage from the Fe-SMA's ability to shrink when heated. After that, mainly plastic deformation occurs. A lower prestrain would reduce the amount of recovery stress as well as the prestress level achieved after activation and, on the other hand, a higher prestrain would shorten the plastic plateau of Fe-SMA material before its rupture.

An AC/DC current transformer used to supply the electrical power, with a relatively high current density of ~ 4.0 A/mm^2 in order to shorten the heating phase and reduce the heat flow into the non-activated Fe-SMA strip zones. Metallic clamps were attached to the Fe-SMA strip at the ends of the activation region (at the same distance from the mid-span section to guaranty post-tensioning symmetry). A circuit was created when the electrode holder and the ground clamp were connected to these metal clamps, with electrical current flowing from the former to the latter.

- **Series S1: monolithic beams**

In monolithic beams, the activation length was set to 700 mm (half of the beam span), creating an undamaged bond length of 400 mm at both beam ends. As the tests on monolithic beams aimed to assess the influence of activation temperature (T_a) on the overall behaviour of Fe-SMA strengthened glass beams, different values were adopted, namely: (i) 120 ºC for the MB_T120 beams, (ii) 140 ºC for the MB_T140 beam, and (iii) 160 ºC for the MB_T160 beam.

- **Series S2: laminated glass beams**

In large beams, due to the surface flaws in glass edges, only the CFRP laminate installed in the groove was prestressed. After being mechanically anchored at both ends using metal clamps, the NSM-CFRP laminate was

stretched up to an average strain of 0.2 % using a hydraulic jack. The axial strain was recorded by means of a strain gauge previously installed in the middle of the CFRP laminate.

A similar strategy was adopted to activate the Fe-SMA reinforcement in the laminated glass beams. Its activation length was set to 1400 mm. The Fe-SMA strips were heated at different temperatures: (i) 180 ºC for NSM-SMA strips; and (ii) 120 ºC for EBR-SMA strips.

2.4. Bending tests

Fig. 3 shows the test setups adopted in this study: all beams were tested adopting a four-point bending configuration, with spans varying between 1.4 m for series S1 and 2.8 m for series S2; load points were 460 mm or 700 mm apart, respectively. To avoid the direct metal-glass contact and premature glass rupture, Teflon plates were always positioned between the steel pieces and the glass. As shown in Fig. 3, due to the slenderness of glass beams, two pairs of vertical metallic guides were used to prevent lateral displacements (e.g. lateral-buckling effect). Also in this sense, tailor-made metal frames were used as supports. Threaded screws were inserted into their holes and slightly pressed against the glass to maintain the alignment of the specimens during the test. LVDT1 and LVDT3 measured the deflections at loading point sections, while the LVDT2 measured the mid-span deflection. Axial strains were recorded through strain gauges placed on the top edge of the glass (SG1) and on the bottom edge of the EBR reinforcement (SG2). Due to the sudden failure of glass, the applied load and deflections were measured using an acquisition frequency of 50 Hz. All tests were conducted in laboratory environment at an average temperature of 24 ºC and relative humidity of 65 %. All experimental tests were also monitored adopting the Digital Image Correlation (DIC) technique, to document the crack evolution and complement the understanding of the structural behaviour obtained from flexural tests until failure. As opposed to the monolithic beams, the region of interest (ROI) of laminated glass beams included only half of the span due to the large dimension of such specimens. As the cracks have propagated symmetrically towards the supports, the crack patterns of laminated glass beams were subsequently mirrored to promote a better overall understanding of experimental response.

3. Results and discussion

Due to the reverse transformation from martensite to austenite, the monolithic beams deformed upwards (pre-camber) between 0.433 and 0.573 mm. As expected, the higher the activation temperature the greater such deformation. Regarding the laminated glass beams, the cumulative pre-camber in the LB_SMA-CFRP beam (SMA activation plus CFRP prestressing) was 0.954 mm, while the upward deformation in LB_CFRP-SMA was 0.552 mm.

Fig. 3 and Fig. 4 show the responses in terms of the applied load (F) *versus* mid-span deflection (δ) for the monolithic and laminated beams, respectively, as well as the crack patterns obtained using the DIC technique before failure. Table 2 includes the main results obtained from these curves of series S1, namely, initial stiffness (K), cracking load (F_{cr}) and corresponding deflection (δ_{cr}), maximum load (F_{max}), ultimate deflection (δ_{ult}), ductility index at failure (Di) defined as the δ_{ult} / δ_{cr} ratio, and residual strength index (RSi) defined as the F_{max} / F_{cr} ratio. Table 3 includes the main results obtained from these curves of series S2. This table includes similar parameters to those of Table 2 and also the ultimate load (F_{ult}).

All beams maintained their integrity after crack initiation. Their structural behavior consisted of two different stages: (i) the pre-cracking stage, where the structural response was mainly governed by the elastic properties of the glass panel; and (ii) the post-cracking stage, where the structural response was significantly influenced by reinforcement properties and composite action provided by adhesive layer. Before crack initiation, all beams presented similar structural responses, exhibiting linear behavior. Subsequently, successive sudden load drops occurred due to the formation of new cracks towards the supports, as well as the propagation of existing cracks towards the top edge of the glass panel (pure bending zone) and the load points (shear cracks), creating non-linear branches with progressive loss of stiffness due to the yielding of the Fe-SMA.

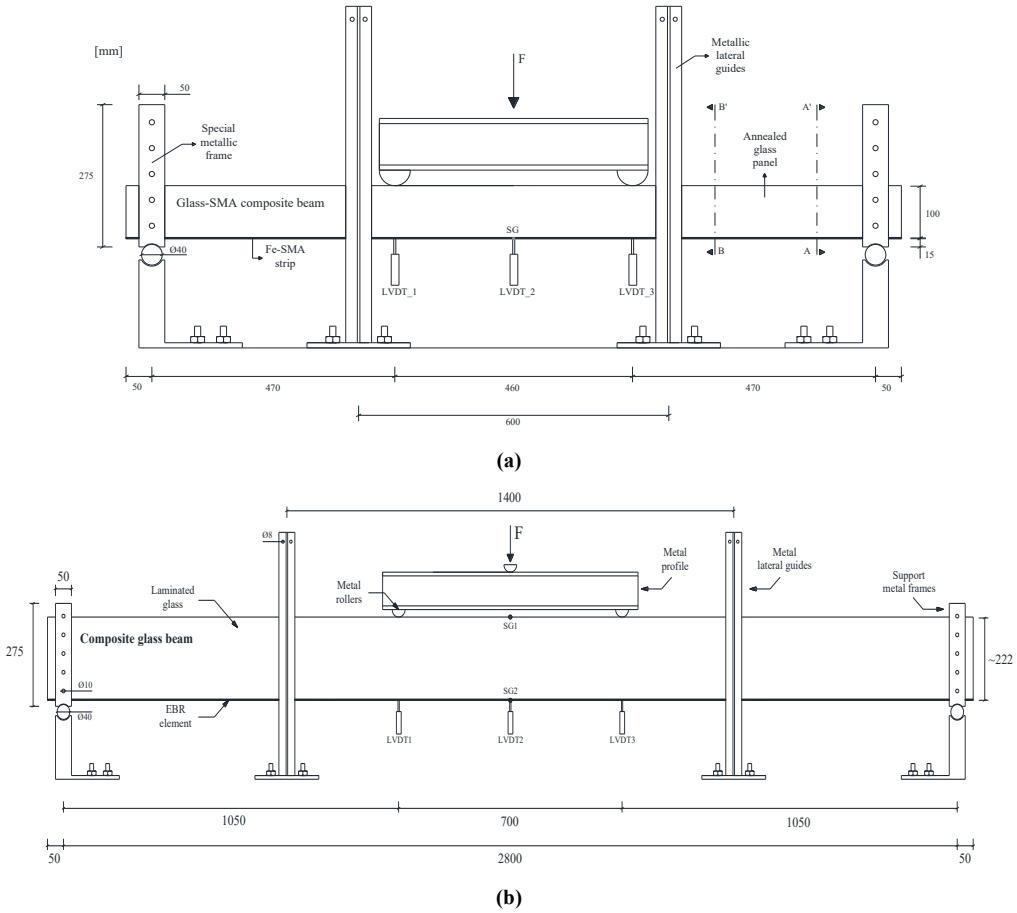

Fig. 3. Four-point bending tests carried out in this study: (a) monolithic glass beams (series S1); (b) laminated glass beams (series S2).

These results also show that the secondary load-carrying mechanism generated after crack initiation, consisting of a compression force in the upper zone of the glass panel and a tensile force in the reinforcement element, led to ductile responses. Thereafter, monolithic glass beams were unloaded before collapse or failed by debonding of the Fe-SMA strip at the reinforcement/adhesive interface, while laminated glass beams ruptured when explosive failure occurred at the compression zone of glass beams.

Excluding the MB_T160 beam, probably due to a large adhesive damage propagation towards the beam extremities resulting in lower camber than expected, all monolithic post-tensioned beams showed lower initial stiffness than the reference ones, varying between 1.8 % (MB_P120 beam) and 2.7 % (MB_T140 beam). This is explained by two main aspects: (i) first, adhesive layer was damaged when heating the Fe-SMA, reducing the composite action between adherends; and (ii) second, the tensile stiffness of the Fe-SMA decreased after activation (Shahverdi *et al.* 2018).

Comparing the post-tensioned monolithic beams to the reference ones, the glass fracture strength was increased between 16.8 % and 30.3 %. However, using inverse analysis, cracking loads were not as high as expected. Despite the inherent variability of the tensile strength, the stress relaxation of the Fe-SMA material seems to be the main reason for such loss of post-tensioning (e.g. Shahverdi *et al.* 2018), which varied between 6.8 % (MB_T120-I beam) and 8.4 % (MB_T140 beam).

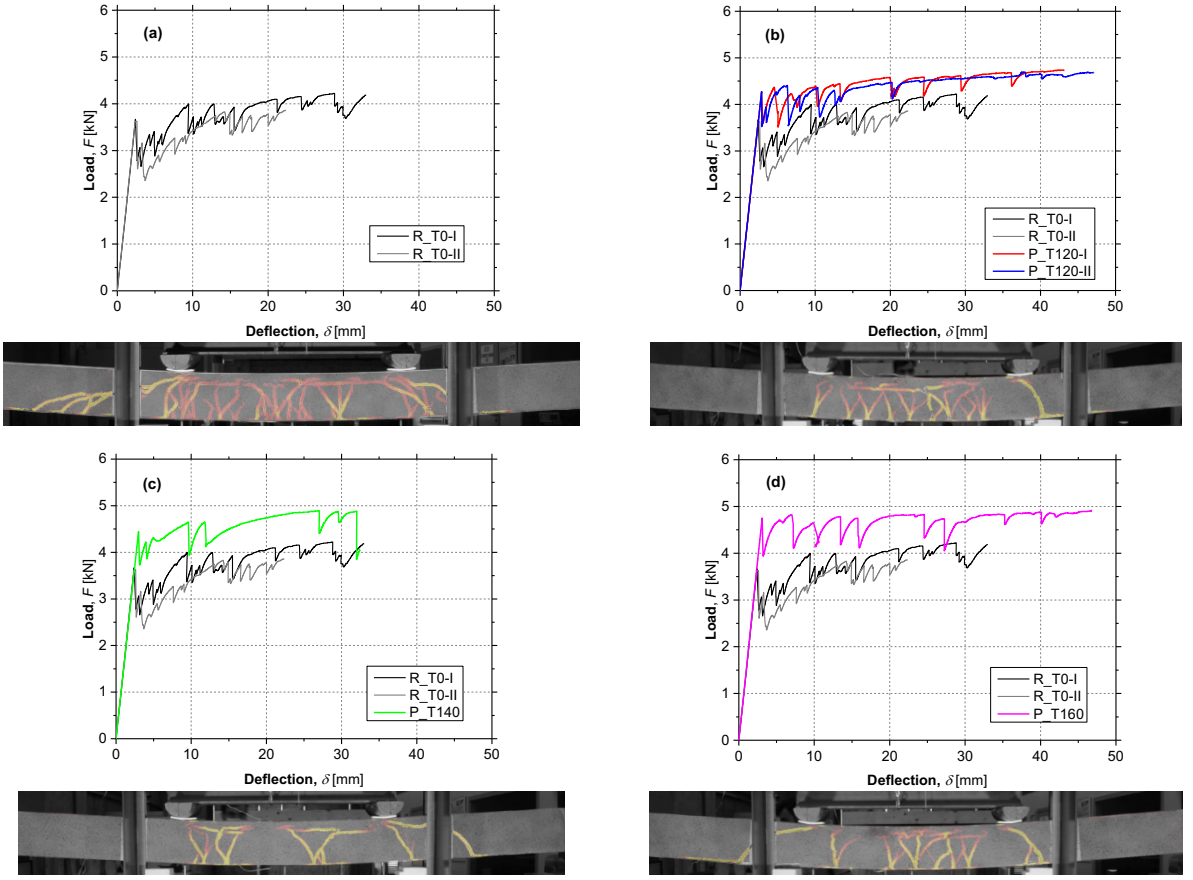

Fig. 4. Series S1: experimental responses and correspondent crack patterns captured before collapse of (a) the reference beams, (b) the MB_T120 beams; (c) the MB_T140 beam and (d) the MB_T160 beam.

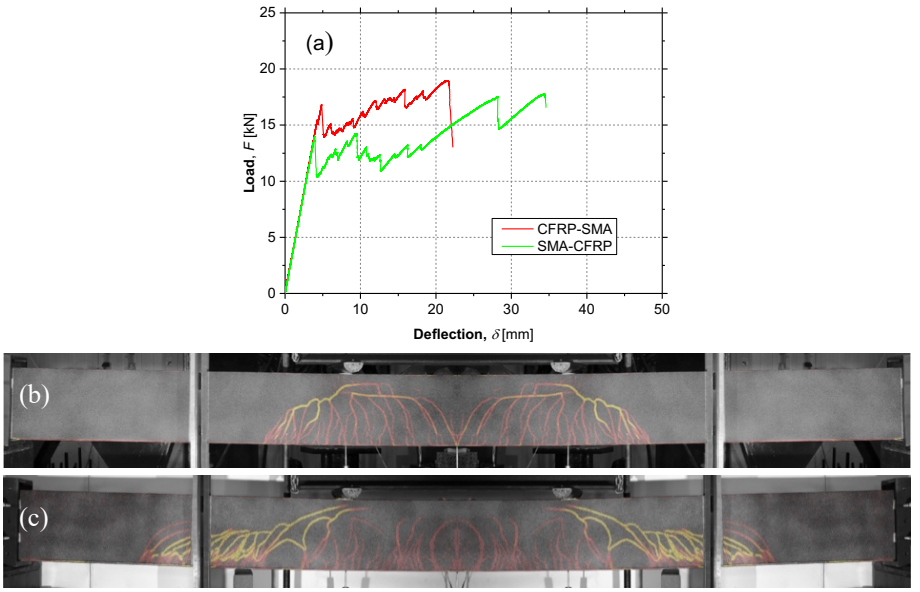

Fig. 5. Series S2: (a) flexural responses of both laminated glass beams; and crack patterns of the (b) LB_CFRP-SMA and (c) LB_SMA-CFRP beams captured through DIC technique before their collapse.

Table 2. Main properties of the reference and post-tensioned monolithic glass beams obtained from the flexural tests (Series S1).

Beam	T_a [ºC]	K [kN/mm]	F_{cr} [kN]	δ_{cr} [mm]	F_{max} [kN]	δ_{ult} [mm]	Di [%]	RSi [%]
MB_T0-I	--	1.53	3.67	2.40	4.22	32.9	1370	115
MB_T0-II	--	1.53	3.63	2.38	3.86	22.1	931	106
MB_T120-I	122	1.50 (-1.8%)	4.26 (16.8%)	2.84 (19.0%)	4.74 (17.2%)	43.2 (56.8%)	1519 (31.9%)	111 (0.4%)
MB_T120-II	124	1.50 (-1.9%)	4.28 (17.2%)	2.86 (19.5%)	4.69 (16.2%)	47.1 (71.0%)	1648 (43.2%)	110 (-0.8%)
MB_T140	142	1.49 (-2.7%)	4.44 (21.8%)	2.99 (25.2%)	4.89 (21.1%)	32.5 (17.8%)	1085 (-5.7%)	110 (-0.6%)
MB_T160	161	1.54 (0.7%)	4.75 (30.3%)	3.09 (29.5%)	4.92 (21.7%)	46.8 (70.0%)	1512 (31.5%)	103 (-6.6%)

Notes: the values indicated in parentheses represents the difference between the properties of the post-tensioned beams with the one of the 'mean' reference beam.

Table 3. Main properties of the laminated glass beams obtained from the flexural tests (Series S2).

Beam	K [kN/mm]	F_{cr} [kN]	δ_{cr} [mm]	F_{max} [kN]	F_{ult} [kN]	δ_{ult} [mm]	Di [%]	RSi [%]
LB_CFRP-SMA	3.63	15.48	4.26	18.95	18.95	22.24	521.7	122.4
LB_SMA-CFRP	3.57	14.02	3.93	17.79	17.79	34.59	881.2	126.9

Post-tensioned beams showed lower F_{max} / F_{cr} ratio*s* than the reference ones. Excluding the MB_T140 beam, probably due to premature glass breakage, their residual strength was lower the higher the activation temperature. This occurred because activating the Fe-SMA reinforcement reduces its tensile strength reserve (difference between σ_{rev} and σ_{rec}) before the forward transformation, thus reducing the post-cracking stiffness of the post-tensioned beams and their load carrying capacity. Therefore, unsafe failures can occur when this tensile strength reserve is not sufficient. Two strategies can be adopted to overcome this challenge: (i) jointly apply another reinforcement material capable of providing stiffness after Fe-SMA yielding or (ii) estimate the maximum recovery stress capable of guaranteeing $F_{ult} > F_{cr}$ and/or increase the reinforcement ratio to obtain the desired post-tensioning applying a lower activation temperature. The latter does not take advantage from major benefit of applying Fe-SMA reinforcement and presents obvious aesthetic impacts.

Consequently, hybrid strengthening systems using Fe-SMA and CFRP materials as reinforcement were explored. Although passive beams have not be tested, their cracking load can be easily estimated from inverse analysis. Considering a cracking load of ~11.40 kN in the case of passive beams (analytical value obtained assuming linear elastic behaviour for all components and assuming the Euler-Bernoulli hypothesis), the glass fracture strength was increased between 24.1 % (LB_SMA-CFRP beam) and 37.0 % (LB_CFRP-SMA beam) due to the post-tensioning. Despite a slight reduction in the reinforcement ratio from 1.25 % (monolithic beams) to 1.08% (laminated glass beams) the *RSi* increased from 111 % to 122 %, at least. Such results indicate that the post-cracking performance of glass composite systems can be significantly enhanced when all or part of the tensile reinforcement is applied according to the NSM technique.

Fig. 4 shows that the position chosen for each reinforcement material played an important role in the post-cracking response, as large beams exhibited different post-cracking responses. Many load drops occurred in the LB_SMA-CFRP beam when $\delta \approx 9.5$ mm (see Fig. 4) because of the sudden formation of shear cracks towards one of the supports. Minor deviations in the beam height were observed (≈ 1.5 %), but they probably occurred in the other laminated glass beam as well. The low tensile stiffness of Fe-SMA after activation made it unable to restrain the crack opening, promoting damage concentration and, therefore, high interfacial stress (mixed mode-I+II fracture) between the CFRP reinforcement and the glass substrate. As additional shear cracks formed in the non-activation region, the strengthening system shifted to a passive-like behavior (no post-tensioning effect), which explains the difference between the ultimate load capacity in both beams. In contrast, the LB_CFRP-SMA beam showed a constant post-tensioning effect on its experimental curve. As CFRP presents linear elastic behavior until failure, as it was prestressed, the increment of loading carrying capacity was approximately constant throughout the post-cracking stage. Therefore, stiffer materials should be used as NSM reinforcement to strengthen glass beams.

Strengthening systems show great difficulties in restraining crack opening when NSM systems are not adopted (e.g. monolithic glass beams) or flexible materials are used as reinforcement (e.g. Fe-SMA after activation).

Conclusions

The experiments conducted showed that it is possible to design and implement strengthening systems that restrain brittle failure in glass structural elements. The beams maintain their integrity after crack initiation and sustain the shock load resulting from cracking and the low fracture energy of glass. All of them collapsed under higher loads after significant deformation. The F_{max} / F_{cr} ratio ranged between 1.03 in monolithic beams and 1.26 laminated glass beams, while the δ_{ult} / δ_{cr} ratio varied between 5.2 in laminated glass beams and 16.5 in the other ones. Compared to the EBR system, the laminated glass beams were more efficient in providing load-carrying capacity after cracking and delaying the premature debonding of the strengthening, observed in monolithic glass beams before collapse.

Monolithic glass beams showed that the F_{max} / F_{cr} ratio strongly depends on the recovery stress on the Fe-SMA reinforcement, which reduces the tensile strength reserve before yielding. Even activated at 120 ºC, the capacity of Fe-SMA to provide stiffness strongly lowers. Despite all advantages of Fe-SMA for applying mechanical prestressing in glass, safety may be compromised because glass beams cannot recovery from the crack initiation. As CFRP is stiffer than Fe-SMA after activation, the results obtained suggest that both materials should be combined because the Fe-SMA is interesting for increasing cracking load while CFRP contains crack propagation due to its high stiffness.

Although further testing is needed, notably glass may be designed to perform as a structural material, and strengthened structural elements made of glass are well within the reach of engineering design in the present or near future.

Acknowledgements

The first author wishes to acknowledge the grant SFRH/BD/122428/2016 provided by Fundação para a Ciência e a Tecnologia, IP (FCT), financed by European Social Fund and by national funds through the FCT/MCTES. This work was partly financed by FCT / MCTES through national funds (PIDDAC) under the R&D Unit Institute for Sustainability and Innovation in Structural Engineering (ISISE), under reference UIDB/04029/2020 (doi.org/10.54499/UIDB/04029/2020), and under the Associate Laboratory Advanced Production and Intelligent Systems ARISE under reference LA/P/0112/2020. Finally, the authors also like to thank the COVIPOR – Companhia Vidreira do Porto Lda., S&P Clever Reinforcement Iberica Lda., SIKA and re-fer AG Company for supplying the materials.

References

Asgarian B, Moradi S. Seismic response of steel braced frames with shape memory alloy braces. J Constr Steel Res 2011;67:65–74.

CNR-DT 2010/2013. Guide for the Design, Construction and Control of Buildings with Structural Glass Elements. CNR - Advis. Comm. Tech. Recomm. Constr., Rome: National Research Council of Italy; 2013.

Cruz P, Pequeno J. Structural Timber-Glass Adhesive Bonding. Challenging Glas., 2008, p. 205–14.

Dong Z, Klotz UE, Leinenbach C, Bergamini A, Czaderski C, Motavalli M. A novel Fe-Mn-Si shape memory alloy with improved shape recovery properties by VC precipitation. Adv Eng Mater 2009;11:40–4.

Ghafoori E, Hosseini E, Leinenbach C, Michels J, Motavalli M. Fatigue behavior of a Fe-Mn-Si shape memory alloy used for prestressed strengthening. Mater Des 2017;133:349–62.

Hosseini A, Michels J, Izadi M, Ghafoori E. A comparative study between Fe-SMA and CFRP reinforcements for prestressed strengthening of metallic structures. Constr Build Mater 2019;226:976–92.

Hosseini E, Ghafoori E, Leinenbach C, Motavalli M, Holdsworth SR. Stress recovery and cyclic behaviour of an Fe-Mn-Si shape memory alloy after multiple thermal activation. Smart Mater Struct 2018;27.

Jordão S, Pinho M, Martin J, Santiago A, Neves L. Behaviour of laminated glass beams reinforced with pre-stressed cables. Steel Constr 2014;7:204–7.

Louter C, Belis J, Veer F, Lebet J. Structural response of SG-laminated reinforced glass beams; experimental investigations on the effects of glass type, reinforcement percentage and beam size. Eng Struct 2012;36:292–301.

Louter C, Cupać J, Debonnaire M. Structural glass beams prestressed by externally bonded tendons. Glas. Glob. Conf. Proc., Philadelphia, EUA: 2014, p. 450–9.

Martens K, Caspeele R, Belis J. Development of composite glass beams - A review. Eng Struct 2015;101:1–15.

prCEN/TS 19100-1:2021. Structural glass – Design and construction rules – Part 1: Basis ofdesign and materials. CEN - Eur. Comm. Stand., 2021.
Rocha J, Pereira E, Sena-Cruz J. Feasibility of mechanical post-tensioning of annealed glass beams by activating externally bonded Fe-SMA reinforcement. Constr Build Mater 2023;365.
Rocha J, Sena-Cruz J, Pereira E. Influence of adhesive stiffness on the post-cracking behaviour of CFRP-reinforced structural glass beams. Compos Part B Eng 2022a;247.
Rocha J, Sena-Cruz J, Pereira E. Tensile behaviour of CFRP-glass adhesively bonded connections: double-lap joint tests and numerical modelling. Eng Struct 2022b;260:114212.
Shahverdi M, Michels J, Czaderski C, Motavalli M. Iron-based shape memory alloy strips for strengthening RC members: Material behavior and characterization. Constr Build Mater 2018;173:586–99.
Silvestru V, Deng Z, Michels J, Li L, Ghafoori E, Taras A. Application of an iron-based shape memory alloy for post-tensioning glass elements. Glas Struct Eng 2022;7:187–210.
Silvestru V, Deng Z, Michels J, Taras A. Enabling a Ductile Failure of Laminated Glass Beams with Iron-Based Shape Memory Alloy (Fe-SMA) Strips. Int. Colloq. Stab. Ductility Steel Struct., Aveiro, Portugal: Ernst & Sohn GmbH; 2022.
Valarinho L, Correia JR, Branco F. Experimental study on the flexural behaviour of multi-span transparent glass-GFRP composite beams. Constr Build Mater 2013;49:1041–53.
Veer FA, Rodichev YM. The structural strength of glass: Hidden damage. Strength Mater 2011;43:302–15.
Wüest T, Luible A. Glass Design in Switzerland. Challenging Glas. 7 - Conf. Archit. Struct. Appl. Glas., Ghent, Belgium: 2021.